Application of Small Angle and Wide Angle X-ray Scattering (SAXS and WAXS) in heterogeneous catalysis and prospects

Qianshan Feng s4650271

Supervised by Prof. Dr. Giuseppe Portale

Contents

Abstract

This review gives a brief description of the most sensible information obtained from x-ray scattering techniques represented by SAXS and WAXS, and also analyzed the most applicable systems for these characterization techniques accordingly. The analysis combines the application of theories and the examples from their most common applications, polymers. Then the typical examples of their application in catalysts materials are analyzed also in terms of the possible information to obtain. Finally the prospect of further application in catalysis processes and heterogeneous catalysts is reasonably predicted.

Introduction

Small Angle and Wide Angle X-ray Scattering (SAXS and WAXS), belonging to total scattering techniques, works on a similar principle with X-ray diffraction, both utilizing the scattering behavior of X-ray beam to probe the distribution of electron density and thus obtain spacial structural information of the probed object. Whereas the signals depend on the lattice sum of the scattering intensity in X-ray diffraction, X-ray Scattering spectroscopy can give information through much less repeated unites than a single crystal, in other words, upon low crystallinity, at a much larger sample size and thus also work well in liquid phase or for soft materials and polymers. In fact, the main application of X-ray Scattering has been centered on polymers for years. [1] Unlike diffraction spectroscopy, which focuses on the position of Bragg peaks representing a few lattice planes, in total scattering spectroscopy, the scattering intensity is taken as continuous and sum over all isotropic scattering entities in a homogeneous sample, to provide information on a long-range scale like surface, size and shape of crystalline particles and the correlation between them. [2]

Heterogeneous catalysts are widely of interest because it's easier to control and separate. In the synthesizing process of catalysts, the design of active sites and spacial structure are determining factors for catalyzing efficiency and often the challenges. In the catalyzing process, the monitoring of the configuration transform in real time and in situ is crucial for understanding the mechanism and thus instructs the design of catalysts. Both of these processes need detailed information about the surface of catalyst particles at a nanometer scale and in real time and environment. [3]

Nowadays the main characterization techniques include XRD for identification, electron microscopy (SEM and TEM) for morphology and size, Raman spectroscopy and IR for binding with reagents and transition species, and X-ray absorption spectroscopy (XANES, EXAFS) for valence and local environment at atomic scale. Due to the environment of chemical reactions (reagents, liquid phase, etc.), the in-situ, operando and high resolution characterization remains challenging. As a consequence, data about the mechanism of the growth, catalyzing and deactivation processes is in deficiency, which may greatly help the evaluation and future development of catalysts.

SAXS and WAXS has already been in use for nanoparticles for years, which is the main form of heterogeneous catalysts. Due to the noninvasive nature of X-ray spectroscopy, there is great facility in its in situ operation in real reaction environments and especially special environments such as high pressure, high temperature and microwave. G. A. Tompsetta et al. monitored the growth of zeolites using the combination of SAXS and Raman spectroscopy. [4] It also provides flexibility to be combined with other characterization techniques such as Raman spectroscopy, IR, X-ray absorption spectroscopy, etc. [1]

Information offered by X-ray scattering spectroscopy

1. Working principle of SAXS and WAXS

The scattered X-ray beam gives information in reciprocal space, where two scattering entities separated apart by *r* contribute to the intensity in the form of e^{iQr} ($Q=4\pi sin\theta/\lambda$, is the wave vector transfer, θ is the scattering angle). Bigger features on a longer range has a big distance *r* which leads to a small limit of wave vector transfer *Q* or scattering angle θ beyond which the beams completely scatter out of phase. So outline information about crystal domains, for example, the surface, shape, size of nano-particles and the interaction between them, only survives in a low angle or small Q *of* $<1Å^{-1}$. This part of total scattering spectroscopy is called Small Angle X-ray Scattering spectroscopy (SAXS). Wide Angle X-ray Scattering spectroscopy (WAXS) covering the range from $Q<1Å^{-1}$ to $Q>10Å^{-1}$ contains information about the arrangement of atoms in the highly dispersed crystalline domains.

2. PDF analysis of SAXS

The most universal analyzing method for scattering techniques is atomic pair distribution function (PDF) analyzing, which directly converts the scattering intensity function *I(Q)* into the electron density function *i(r)* around one core through Fourier transform [5], as shown by (1)(2) for SAXS [6].

$$\mathrm{I(Q)} = 4\pi \int_0^\infty i(r)\frac{\sin Qr}{Qr}dr \quad (1)$$

$$i(r) = p_0(r, R_s) + \int_0^\infty \tilde{p}\,(r, R_s, a)h(a)\frac{3\varphi}{4{R_s}^3\pi}4a^2\pi da \quad (2)$$

$p_0(r, R_s)$ is the pair distance distribution function (PDDF) of a single sphere as a function of *r* and the homogeneous sphere radius R_s. φ is the volume fraction of particles and $\frac{3\varphi}{4{R_s}^3\pi}$ is the particle number density, which multiplying with $4a^2\pi da$, the volume of a spherical shell at an increase of radius *da*, gives the total density in completely disorder. $h(a)$ is the total correlation function, representing the difference of the number of spheres in the shell brought by order. $\tilde{p}(r, R_s, a)$ is the cross-term coming from the finite size of of the particle centred at a distance *a* which causes broadening of the total correlation function $h(a)$. [6]

The first minimum of *i(r)*, corresponding to the zero-point of $p_0(r, R_s)$ when there is no correlations, can be used to estimate the diameter of particles. The estimation gets worse at high concentration or small $p_0(r, R_s)$. The interaction between particles can also be deduced from *i(r)*. Strong repulsion can bring severe lowering of the first minimum and shift of its position to a bigger *r*, which also brings a kink as an indication of the radius in the place of the original first minimum. Conversely, attraction or screened charge make the first minimum shallower and shifts its position to a smaller *r*, which is less trivial. [6]

With a pseudo-crystalline or super lattice structure caused by the assembly of particles, there is strong oscillations in *i(r)* extended to a very big *r*, with peak positions as analogy to Bragg peaks. In this case the positions of the peak can give the positions of neighboring particles in the real space, otherwise the peak position doesn't directly equal the distance between particles although can act as an indication of nearby particles.

3. Form factor and structure factor

The pair distance distribution function *p(r)* is related to the form factor *P(Q)* through Fourier transform.

$$\mathrm{P(Q)} = 4\pi \int_0^\infty p(r) \frac{\sin Qr}{Qr} dr \quad (3)$$

Likewise, the correlation function *h(r)* is also related to the structure factor S(Q) through Fourier transform.

$$\mathrm{S(Q)} = 1 + 4\pi \mathrm{n} \int_0^\infty h(r) r^2 \frac{\sin Qr}{Qr} dr \quad (4)$$

n is the particle number density.

$$\mathrm{n} = \frac{N}{V}$$

$$\mathrm{I(Q)} = \mathrm{n} V_p^2 |\Delta\rho|^2 P(Q) S(Q) \quad (5)$$ [2][6]

4. Porod's Law and Guinier Law

Apart from size and distribution, another most commonly obtained information is surface roughness of scattering entities. The differential scattering cross section follows a power law of Q. [2][8]

$$\lim_{Q\to\infty} \frac{d\sigma}{d\Omega} = I(Q) = 2\pi |\Delta\rho|^2 S_V Q^{-x} \quad (5)$$

$$|\Delta\rho|^2 = |\rho_s - \rho_m|^2 = r_e^2 \langle f \rangle^2 \quad (6)$$

S_V is the surface area per unit volume. $|\Delta\rho|$ is the excess scattering intensity of the particle ρ_s after the subtraction of the environment ρ_m. r_e is the scattering length of a single electron also known as Thompson radius. $\langle f \rangle^2$ is the mean square atomic factor.

For a smooth surface, the power x is 4 and when surface roughness increase, the power x decrease to <4. The regime that this law is applicable is called Porod Regime, which requires $Qr>10$, $Q \lesssim 0.1 Å^{-1}$, usually at the tail of the SAXS curve.

Guinier Law is used at low *Q* values for extension or interpolation of the SAXS curve

to below the Q resolution. [5][8]

$$\mathrm{I(Q)} = (\rho V)^2 \exp\left(-\frac{(QRg)^2}{3}\right) \quad (7)$$

$$\ln(\mathrm{Q}) = \ln(\rho V)^2 - Q^2 \frac{R_g^2}{3} \quad (8)$$

R_g is the gyration radius and $QR_g<1$.

5. WAXS and Extended Range-PDF analysis(ER-PDF)

The signal from WAXS, usually covering the Q range from 0.5 $Å^{-1}$ to 10$Å^{-1}$ and up to 20 $Å^{-1}$, is more traditionally interpreted by crystal planes corresponding to Bragg peaks. The advantage of WAXS compared with XRD is that the total scattering technic can be used for characterization of low crystallinity domains that are even well-separated by or highly dispersed in amorphous regimes or in liquid environment. For example, WAXS can be used to monitor the growth of crystal particles or the phase transform while XRD needs high degree of crystallinity to show distinguishable signals in solid samples. The angle resolution of WAXS is also bigger than SAXS due to the bigger range. However, it's the maximum Q of WAXS that determines the resolution of real space.

WAXS and SAXS signals can be connected on Q in reciprocal space to give a full-range real-space pair distribution function by performing ER-PDF analysis. Although this analysis doesn't provide more information than separate analysis of the two spectroscopy, it can present more intuitive picture in real space of the micro- to mesoscopic structure of the system. The condition for performing ER-PDF analysis is that the SAXS signal needs to be sufficiently higher than WAXS signal and there need to be an overlap of the Q range. In the overlap region, SAXS signals are used to replace WAXS signal after normalization and leveling because of its smaller (higher) resolution. [2]

J.K.R. Weber et al. performed ER-PDF analysis for the SAXS and WAXS data of nano-alumina, nano-diamond, SBA-15, MCM-41, etc. samples at X-ray Science Division of the Advanced Photon Source of Argonne National Laboratory, USA with Beamline 6-ID-D. [2]

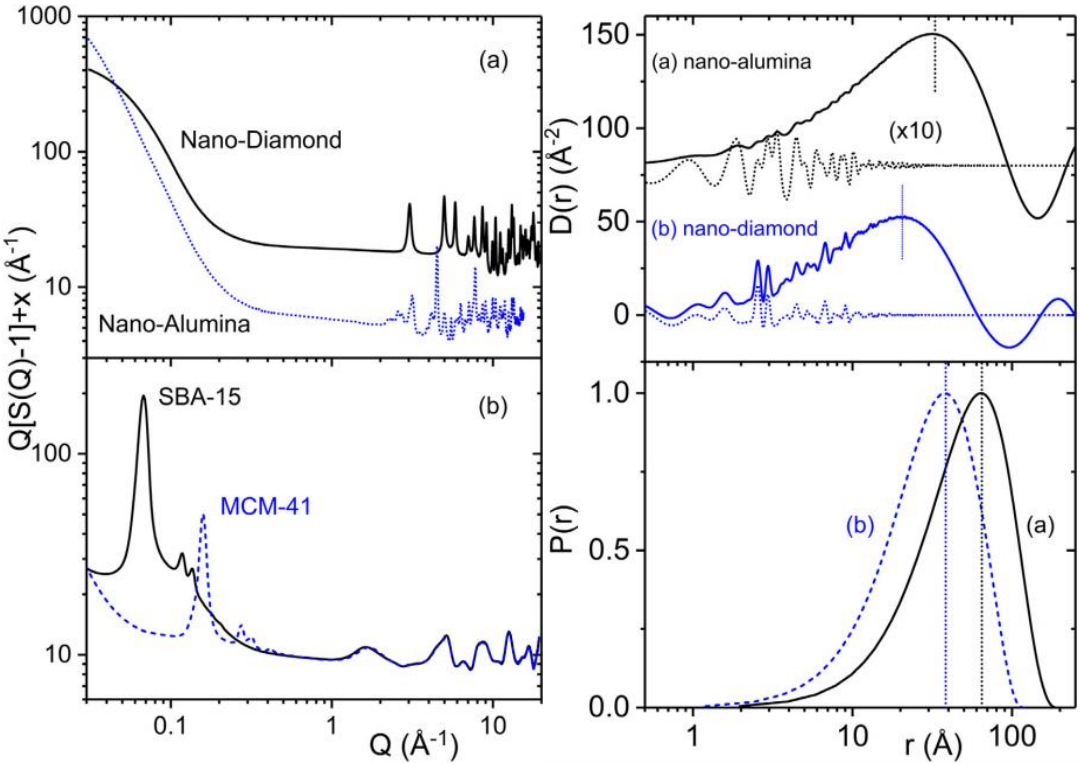

Figure 1 (left). Extended X-ray structure factors for (a) nano-Diamond (solid line) and nano-Alumina (blue dotted line), offset for clarity and (b) amorphous mesoporous silicas SBA-15 (solid line) and MCM-41 (blue dashed line).[2]
Figure 2 (right). Top: The SAXS–WAXS extended range X-ray pair distribution functions of (a)nano-Alumina and (b) nano-Diamond (solid lines) compared to the conventional PDF analysis using WAXS data only (dotted lines, note this curve for nano-alumina has been scaled by x10). Bottom: The PDDF for (a) nano-Alumina (solid line) and (b) nano-Diamond (blue dashed line). The maxima are marked by dotted vertical lines. Reprinted from [2], Copyright (2022), with permission from Elsevier.

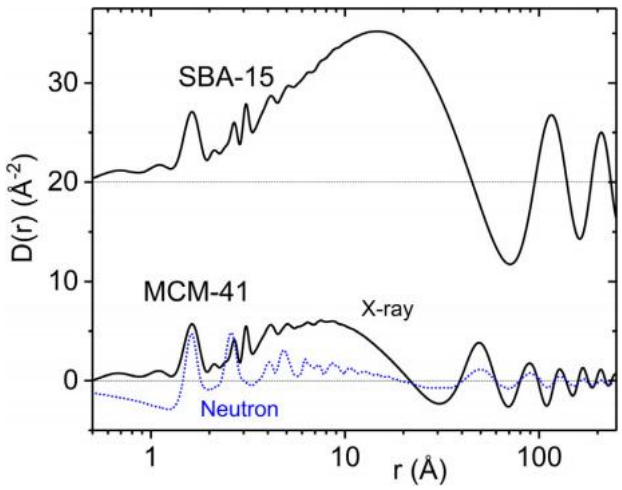

Figure 3. The extended range X-ray pair distribution functions, $D(r)$, for amorphous mesoporous silicas SBA-15 and MCM-41 (solid black curves). In the lower part of

the figure the X-ray MCM-41 is compared to the published neutron pair distribution function for MCM-41 silica from Bowron et al. [9] (blue dotted line, scaled for clarity). Reprinted from [2], Copyright (2022), with permission from Elsevier.

As is shown in Figure 1 to Figure 3, the ER-PDF gives a more intuitive presentation of the distribution of scatter entities and hierarchical structures. The overlap of p(r) of the broad peaks coming from SAXS and Bragg peaks from WAXS also shows the intensity of correlation that is not trivial from WAXS signal itself. ER-PDF also gives better characterization of the particle diameter as compared with TEM pictures. [2]

6. Long-range and low-crystallinity applicable

The most advantageous feature for SAXS and WAXS is their applicability for long-range and low-crystallinity systems. One of the most typical systems is polymer, which is usually composed of small-sized crystalline domains dispersed in amorphous phase. SAXS and WAXS can be used to characterize their crystallinity. Co-polymer building blocks can also form super-structures like lamellar, cylinder, BCC or FCC structures that can be most sensitively captured by SAXS. [10]-[13]

A.J. Ryan and W. Bras et al. used the combination of time-resolved SAXS and WAXS for the degree of crystallinity and its variation with temperature and lamellar thickness of polyethylene on beamline 8.2 of the SRS at the SERC Daresbury Laboratory, Warrington, UK. [10]

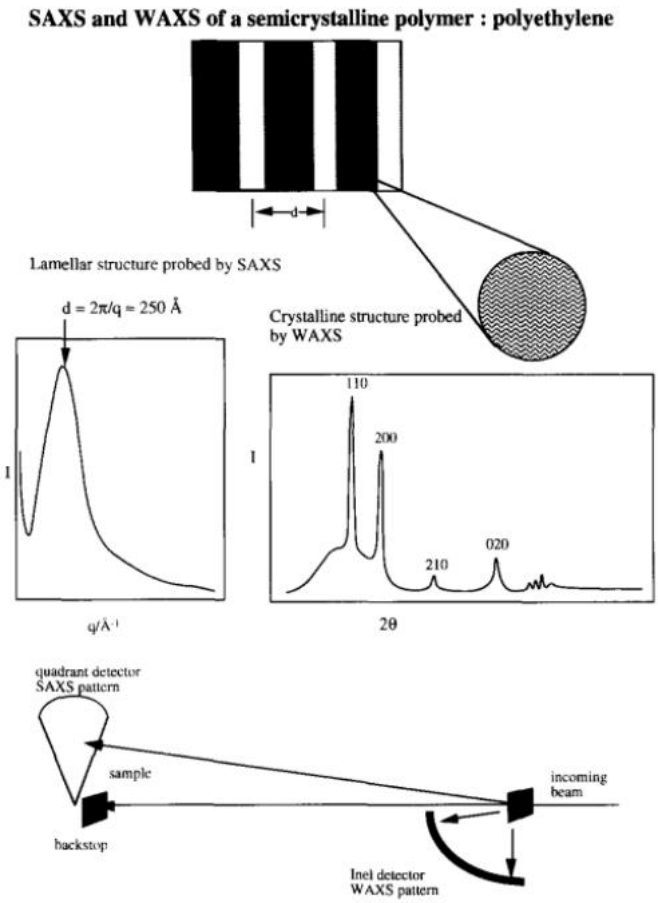

Figure 4. Spatial information available from SAXS and WAXS experiments on semi-crystalline polymers. The SAXS experiments allow calculation of the lamellar spacing from the peak maximum. The crystal structure may be deduced from the positions of the peaks in the WAXS pattern. The camera geometry is also shown. Reprinted from [10], Copyright (2022), with permission from Elsevier.

As is shown in Figure 4, the thickness of the lamellar layer can be obtained from the first peak in SAXS and the crystallinity can be calculated from the ratio of the integrated Bragg peak intensity versus the total intensity integration from WAXS.

7. Time-resolution, Operando characterization and combination with other techniques

Although SAXS and WAXS can be used for low crystallinity, the low scattering intensity still result in bad signal-noise ratio. Therefore, synchrotron source is commonly used because of its brightness, especially for polymers that need a strong penetration. Synchrotron source also provide the possibility for in-situ, time-resolved and operando characterization and the combination with other techniques such as Raman Spectroscopy, Fourier-transform Infrared Spectroscopy (FTIR), Ultraviolet-Visible Absorption Spectroscopy (UV-Vis), Differential Scanning

Calorimetry (DSC) and Differential Thermal Analysis (DTA)
The set up combing multiple techniques and under synchrotron source has been widely used for monitoring the transition processes of polymers with the change in temperature or under strain, etc., which is an important study for industrial processes. [10],[14], [16]-[19]

S.Saidi, G.Portale et al. combined Raman spectroscopy and DSC with time-resolved SAXS and WAXS for the phase transition of PVDF/fluoroelastomer blend with temperature on DUBBLE, BM26, at European Synchrotron Radiation Facility, Grenoble, France. [14]

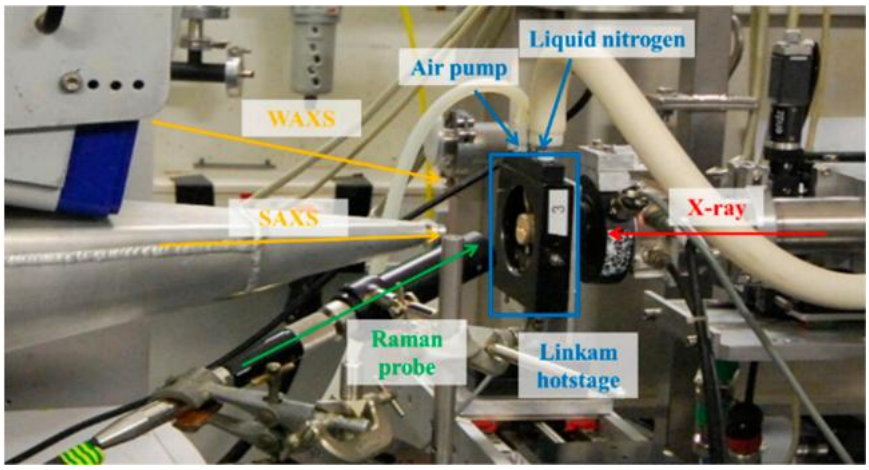

Figure 5. The simultaneous SAXS/WAXS combined with both Linkam DSC and Raman spectroscopy setup at the Dutch-Belgian Beamline (DUBBLE, BM26) at the European Synchrotron Radiation Facility (ESRF). Reprinted from [14], open access.

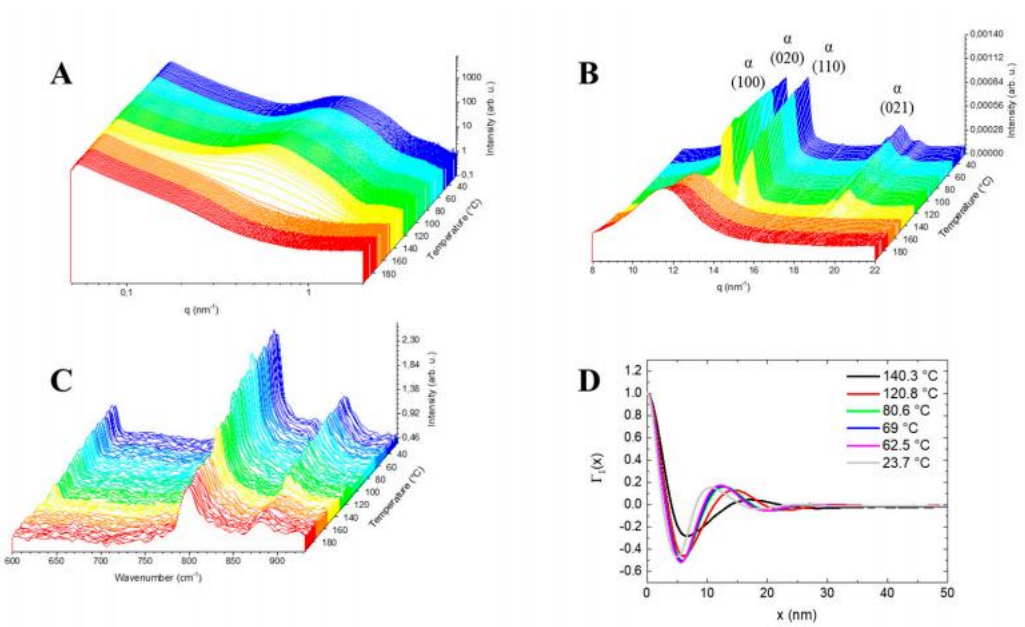

Figure 6. Three-dimensional plots of the time-resolved SAXS (A) and WAXS (B) pattern (100), (020), (110) and (021) (hkl) planes of the monoclinic PVDF phase (pseudo-orthorhombic) [15] and Raman spectra (C), obtained using in situ Raman

spectroscopy combined with SAXS/WAXS coupled to a Linkam DSC setup, during the cooling step from the melt to room temperature (RT) of the blend PVDF/fluoroelastomer sample. (D) Correlation function derived from the SAXS data of the PVDF blend derivative upon cooling. Reprinted from [14], open access.

The setup which combines SAXS, WAXS, Raman Spectroscopy and DSC using synchrotron source to study the phase transition of PVDF/fluoroelastomer blend is shown in Figure 5. Figure 6 shows the phase transition interpreted from the peak evolution with time (temperature). The information of the boundaries of the lamellar layers can also be obtained from the correlation function deduced from SAXS data, so that the crystallization process and the forming mechanism of the lamellar structures can be studied.

Application in catalysis

From the discussions above, it can be observed that X-ray scattering techniques are the most sensitive for systems with a hierarchical structure. Since catalyzed reactions in heterogeneous catalysis mostly happen on the surface and depend on the absorption of reactants on the surface,[3] the more precise characterization of the surface of heterogeneous catalysts is the ultimate goal. The surface features described by X-ray scattering techniques are much larger than atomic bondings but give good description of the outline of entities and the interaction between them. The best applications in catalyzing would be catalysts with secondary structures or processes with a revolution of scattering entities.

1. (Noble) Metal Nanoparticles

(Noble) metal nanoparticles are a class of heterogeneous catalysts. Using SAXS, their behavior can be studied in terms of size and its distribution, shape, surface charge in a in-situ and time-resolved way. Therefore, the crystallization and coalescence behaviors can be captured when monitoring the growth or deactivation processes and thus offer the chance for better explanation of the mechanism. Compared with conventional characterization methods that can provide the information about size, surface and shape, such as TEM and SEM, x-ray scattering techniques can be performed in real time and environment and thus offer more data and avoid the influence of further operations like precipitation and drying. Unlike for polymers, where synchrotron source must be used for high signal-noise ratio, x-ray scattering experiments on metal nanoparticles can be performed by laboratory-based equipment with Cu K α edge beam.

(1) Size distribution and evloution

Cristiano L. P. Oliveira and Matthias Epple et al. performed SAXS for Ag and Cu-Ag bimetallic nanoparticles in wet-chemical reduction synthesis on laboratory–based equipment Xenocs XEUSS™ with radiation generated by a GENIX™ source (Cu K α edge, λ =1.54Å) and the beam focused by FOX2D™ optics. The size distribution

of nanoparticles is added to *I(Q)* using *Monte Carlo (MC) model*, and influence of large aggregates is included to the model by a Guinier Structure Factor (S_G).

$$\mathrm{I(Q)} = \mathrm{B} + S_C(\tfrac{4}{3}\pi)^2 \sum_{i=1}^{N_S} P_i^{sph}(Q, R_i)\, R_i^{(6-pc)} \quad (9)$$

$$S_G(q, R_G) = 1 + S_C^G \exp\left(-\frac{q^2 R_G^2}{3}\right) \quad (10)$$

N_S is the number of spheres accounting for the MC model. The scale factor S_C^G is related to the fraction of aggregates. [20]

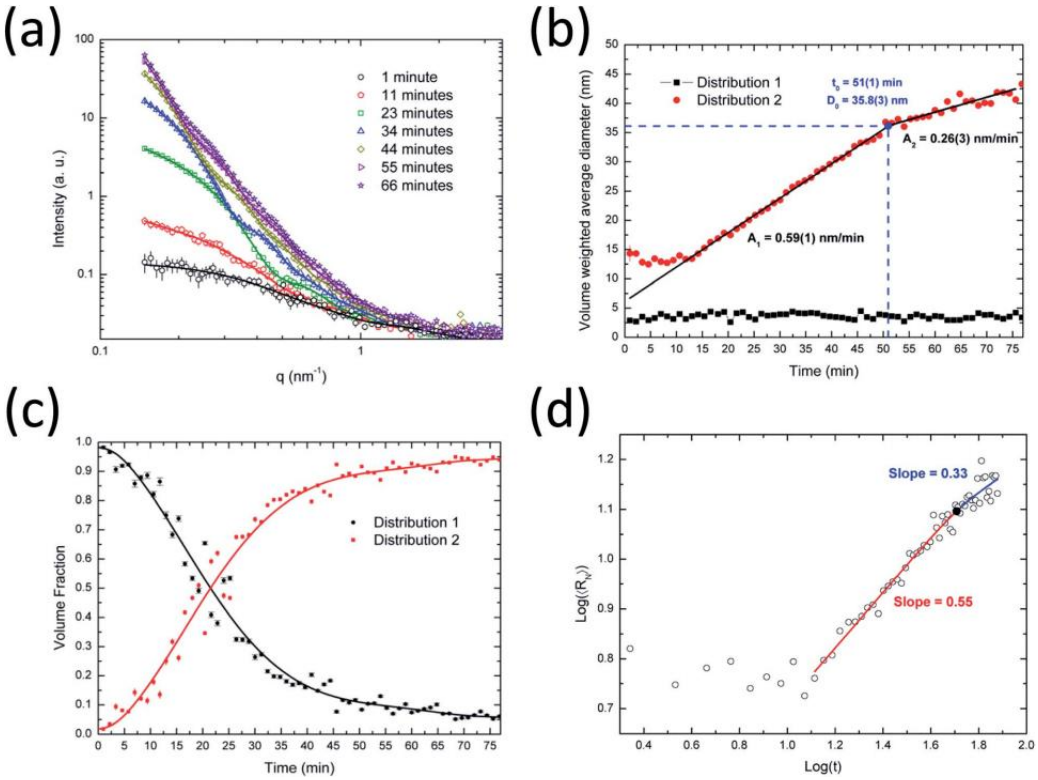

Figure 7. SAXS results for Ag nanoparticle synthesis. (a) Experimental in situ SAXS data (symbols) and theoretical curves (lines) recorded during the synthesis of silver nanoparticles at 90°C, (b) volume weighted average diameter of distributions 1 and 2, (c) temporal evolution of the volume fractions and (d) log–log plot of the number weighted average radius as a function of time. Reprinted from [20], open access.

The coalescence of small crystal grains of 3nm to form an aggregation of 36nm is proved through the temporal evolution of the two size distributions in volume weighted average diameter and volume fraction. The transition of the growth mechanism from coalescence to Ostwald ripening is proved by the growth rate as revealed by Figure 7.(d) of log–log plot of the number weighted average radius as a function of time. The transition point is indicated by the kink in the slope representing the growth rate.

K. M. Ø. Jensen et al. used SAXS for the size distribution of Os nanoparticles with a diameter from 0.3nm to 1.3nm from surfactant-free synthesis using a JJ-XRay

instrument with a Rigaku 100 XL+ micro focus and sealed tube X-ray source (wavelength of 1.54 Å) at Niels Bohr Institute at the University of Copenhagen. They also combined x-ray total scattering with a Q range of up to 21 $Å^{-1}$ and performed PDF analysis for fitting with a *hcp* structure model at beamline 11-ID-B at the Advanced Photon Source, Argonne National Laboratory. [21]

C. Tsao and T. Lin used the indirect transform method [23] and included the interaction of particles using depleted-zone model upon hard sphere model (ITM + HS) to simulate the SAXS intensities of Al-Li alloy during δ' precipitation. They performed SAXS experiment to test the simulation at the X-ray scattering laboratory of the Department of Engineering and System Science, National Tsing Hua University at Hsin-Chu. The X-ray source at this facility is an 18 kW rotating-anode X-ray generator equipped with a Cu target. [22]

More applications on SAXS for nanoparticle size characterization can be seen from [24] to [26]. Although there is already significant development in nanoparticle synthesis that can provide monodispersity in size and all other surface properties in great precision, the information about size distribution and evolution can still be useful for the mechanism of growth or aggregation processes, which are directly related to the production and deactivation of catalysts. Especially for industrial catalyzing processes, where a big amount of samples is present, the in-situ and high-penetration real-time characterization from x-ray scattering techniques can be extremely useful. From the study on precipitation in Al-Li alloy, it can be seen the potential of applying SAXS in supported catalysts, which are composed of metal nanoparticles dispersed on a solid substrate. The fact that x-ray scattering experiments for metal nanoparticles can be performed in laboratory-based setups also provides feasibility for these applications.

(2) Shape and morphology control

i) Inducing form factors

The most common way for fitting SAXS data to certain shape or morphology is using structure factor. P. Mulvaney et al. monitored the growth of nearly monodispersed gold nanorods using in-situ SAXS and tracked its transition from spherical to ellipsoid and then to a spherically capped cylinder. The SAXS experiment was performed at Australian Synchrotron in Melbourne and in combination with UV-Vis absorption spectroscopy. The form factors used for fitting of SAXS data are shown in (11) to (14). [27]

$$\mathrm{I(Q)} = \frac{scale}{V} F(Q)^2 + background \quad (11)$$

$$F(Q)^2 = [3\mathrm{V}(\Delta\rho) \cdot \frac{\sin(Qr) - \mathrm{Qr} \cdot \cos(Qr)}{(Qr)^3}]^2 \quad \text{(Sphere) (12)}$$

$$F(Q)^2 = \frac{3}{V_s}[\mathrm{V}_c(\rho_c - \rho_s) \cdot \frac{\sin(Qr_c) - \mathrm{Qr}_c \cdot \cos(Qr_c)}{(Qr_c)^3} + \mathrm{V}_s(\rho_s - \rho_{solv}) \cdot \frac{\sin(Qr_s) - \mathrm{Qr}_s \cdot \cos(Qr_s)}{(Qr_s)^3}]^2$$

(Core-Shell Sphere) (13)

$$F(Q)^2 = [3V(\Delta\rho) \cdot \frac{\sin\left(Qr(R_p,R_e)\right) - \cos\left(Qr(R_p,R_e)\right)}{\left(Qr(R_p,R_e)\right)^3}]^2 \text{ (Ellipsoid)(14)}$$

For ellipsoid there is $r(R_p, R_e) = [{R_p}^2 + {R_e}^2]^{\frac{1}{2}}$ (15) and $V = \frac{4}{3}\pi(R_pR_e)^2$ (16). R_p is the polar radius along the rotational axis of the ellipsoid and R_e is the equatorial radius perpendicular to the rotational axis.

For spherically capped cylinder, with r as radius and R as cap radius, define $h = -\sqrt{R^2 - r^2} < 0$ when R≥r.

$$I(Q) = \frac{\Delta\rho^2}{V}\langle A^2\langle Q\rangle\rangle \text{ (15)}$$

$$A(Q) = \pi r^2 \frac{\sin\left(\frac{1}{2}QL\cos\theta\right)}{\frac{1}{2}QL\cos\theta} \cdot \frac{2J_1(QL\sin\theta)}{Qr\sin\theta} + 4\pi R^3 \int_{-\frac{h}{R}}^{1} \cos\left[Q\cos\theta\left(Rt + h + \frac{1}{2}L\right)\right] dt \cdot (1 - t^2)\frac{J_1[QR\sin\theta(1-t^2)^{1/2}]}{QR\sin\theta(1-t^2)^{1/2}} \text{ (spherically capped cylinder)(16)}$$

$$F(Q) = V_c(\rho_c - \rho_s)\frac{\sin\left(\frac{1}{2}QL\right)}{\frac{1}{2}QL} \cdot \frac{2J_1QR}{QR} + (\rho_c - \rho_{solv})V_s\frac{\sin\left(Q(\frac{1}{2}L+T)\right)}{Q(\frac{1}{2}L+T)} \text{ (core-shell cylinder)(17)}$$

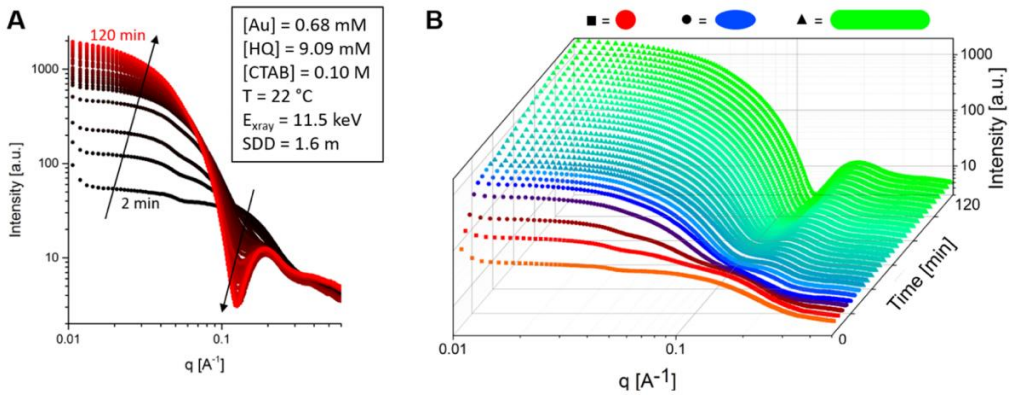

Figure 8.(A) Two-dimensional, time-resolved SAXS intensity as a function of scattering vector q for sample S4. The solid lines in the waterfall plot are fits using a cylindrical form factor. The scattering signal indicates a shift from spherical to rod-shaped particles and an increase in volume overtime. (B) "Waterfall" plot showing the shape transition from sphere (orange to red) to ellipsoid (blue) to a spherically capped cylinder (aqua or green) as a function of the reaction time. The reaction time was 2 h, with spectra collected every 2 min. Reprinted (adapted) with permission from [27]. Copyright 2022 American Chemical Society.

As is shown in Figure 8, the evolution of the gold nanorod from spherical to ellipsoidal and to spherically capped cylinder can be tracked by SAXS with time-resolution. Upon fitting to the cylinder form factor, the length and width can also

be obtained from R_p and R_e. The scattering intensity from the CTAB surfactant at the surface of nanoparticles in colloidal solution is also accounted for by using a form factor with core-shell structure. By fitting the more-shell model to the SAXS data, the thickness of the CTAB layer can be obtained.

ii) Building 3-D models

Instead of fitting the data with form factors, R. Contreras-Caceres et al. built three dimensional models of scattering centers to account for the scattering intensity. As shown in Figure 9, the 3D models consist of 30,000 scattering centers which are enclosed in the morphology of nanotriangles (two bottom connected truncated pyramid). [28]

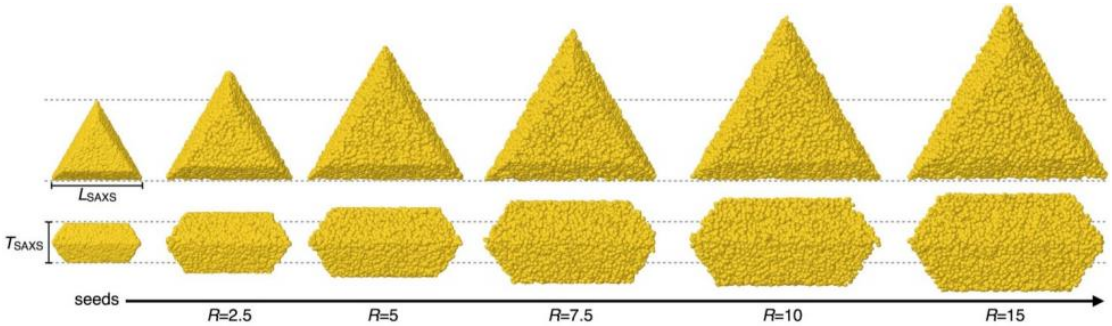

Figure 9. Best-fit SAXS models of ensemble-averaged dimensions for AuNTs before and after gold overgrowth. Each model consists of 30,000 scattering centers, randomly placed within the boundaries set by the idealized NT geometry of a triangular bifrustum. The images were plotted using the van-der-Waals radius of Au. The dashed lines are guides to the eye. Please note that the applied SAXS models also consider the dispersity in edge length and thickness (not shown). Reprinted from [28], open access. Further permissions related to the material excerpted should be directed to the ACS.

The 3D morphology was described by 4 independent parameters, edge length, dispersity in edge length, thickness, dispersity in thickness. The best fit is found by the minima point of mean square error (MSE) compared with experimental data upon the variation of the four parameters. Figure 10 A to F shows the minima in MSE as indicated by the red cross. G and H shows the uncertainty of the analysis, which is less than 1nm for length scales of 70nm-80nm.

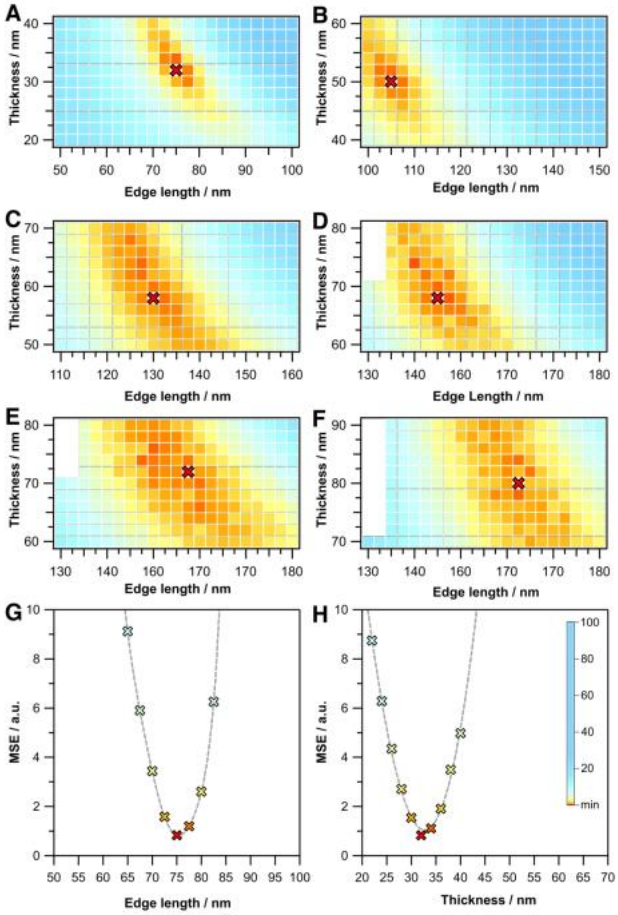

Figure 10. SAXS analysis: MSE maps of AuNTs (A) before and after gold overgrowth: (B) R=2.5,(R indicating the reactant ratio and the size of the nanotriangle) (C) R=5, (D) R=7.5, (E) R=10, and (F) R=15 (logarithmic color scale, see H). The best-fit model,indicated by the lowest MSE, is marked x and highlighted in red color (compare Table 1). The ensemble-averaged NT dimensions can be evaluated with very low uncertainty (<1 nm) because of the high sensitivity of the scattering response: exemplary MSE minima for variation of (G) edge length and (H) thickness for AuNT seeds before overgrowth (cross-sections in A). Reprinted from [28], open access. Further permissions related to the material excerpted should be directed to the ACS.

In this case SAXS gives better description of the sharpness of the edges of the morphology than electron microscope. Although electron microscopes are more commonly used techniques for nanoparticle characterization, small features like sharp edges or vertex are always rounded because of limited resolution and charging effects. However, for SAXS, these features are neither limited by the Q range nor limited by the angular resolution.

More studies on using SAXS for the morphology of nanoparticles can be found in [29] and [30]. A more thorough analysis of SAXS data interpretation for Au nanoparticles can be found in [31].

As can be seen from the second example, the application of SAXS on featuring sharp edges of nanoparticles exceeds other characterization methods. The sharp features can become active sites for catalyst reactions because of the Localized Surface Plasmon Resonances (LSPRs), for example, CO_2 photo-reduction. In real synthesizing experiments, the sharp features are also difficult to obtain. Through the real-time and in-situ monitoring of the growth especially for these features a better guide for reproducing the synthesis can be provided.

2. Framework materials

Framework materials, represented by Metal-Organic Frameworks (MOFs) can not only act as catalysts themselves by the metal linkages or serve as the substrate or precursor of substrate for supported heterogeneous catalysts. However, the synthesis of MOFs are often concerned with uncertainty because of the extreme environment required by the synthesizing methods. For example, the most common hydrothermal or solvent-thermal synthesis need heating and creates high-pressure in the sealed reactor, thus hinders the growth mechanism study. The non-invasive nature of x-ray scattering techniques make them most appropriate for this case.

Gascon, J. et al. combined time-resolved SAXS and WAXS for the growth of NH_2-MIL-53(Al) and NH_2-MIL-101(Al) at the BM16 beamline of the European Synchrotron Radiation Facility, ESRF (Grenoble, France), and X9 beamline at the NSLS in Brookhaven (NY, USA). [32]

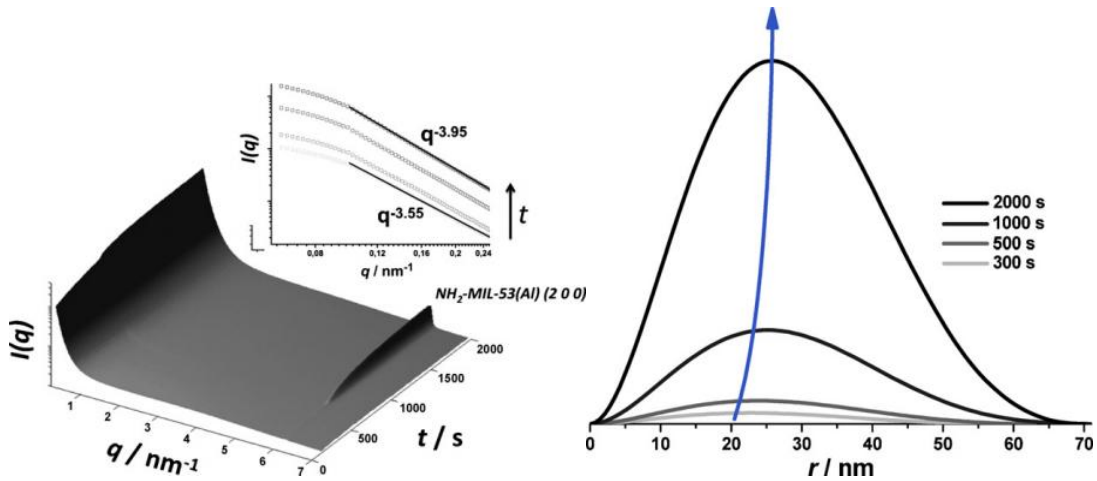

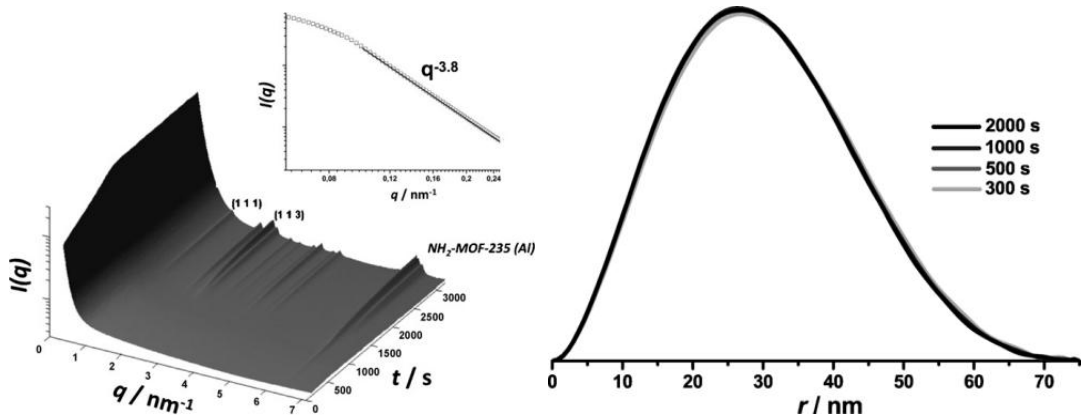

Figure 11a. (top left). Time evolution of the WAXS pattern during the in situ synthesis of NH_2-MIL-53(Al) in H_2O @130 °C, with corresponding SAXS decays in log–log form (inset).
Figure 11b. (top right). p(r) function during the synthesis of NH_2-MIL-53. The blue arrow indicates the increase of intensity and radius of gyration Rg.
Figure 11c. (bottom left) WAXS pattern with the formation of NH_2-MIL-101(Al) in DMF and corresponding SAXS decay (inset).
Figure 11d. (bottom right) p(r) function shows constant scatterer intensity and morphology during formation of NH_2-MIL-101(Al) in DMF, suggesting a slow solid-to-solid conversion. Reprinted from [32], Copyright (2022), with permission from
Elsevier.

From Figure 11a and 11c, the surface roughness of the scattering entity can be indicated from the power of *Q* (*Q* in accordance to the discussion above, q in the figure) according to Porod's Law. The power that is smaller than 4 indicates a rough surface which is typical for porous material. The transition of power in Figure 11a can be interpreted as a two-step growth of porous material, the first step is the smoothening of the surface and the second is densification of internal structure.

The intermediate species can be identified from the evolution of Bragg peaks with time in WAXS data. Compared with NH_2-MIL-53(Al) synthesized in H_2O, NH_2-MIL-101(Al) in DMF has extra peaks standing for the intermediate NH_2-MOF-235 that appear from the very beginning of the growth.
From the *p(r)* functions in Figure 11b and 11d, the increase of intensity indicates the increase of crystallinity which corresponds to the growth of crystal grains. The shift of the peak position can be attributed to the change of local structure, like extension or shrinkage of the linkers, etc.

G. A. Tompsetta et al. interpreted the SAXS and WAXS data in the same way for the growth of zeolites but under microwave synthesis. They also combine Raman spectroscopy to the setup. The experiments were carried out at X10A beamline at Brookhaven National Synchrotron Light Source in Upton, New York. Figure 12a

shows a scheme of the setup. Figure 12b shows the way the waveguide system work. [4]

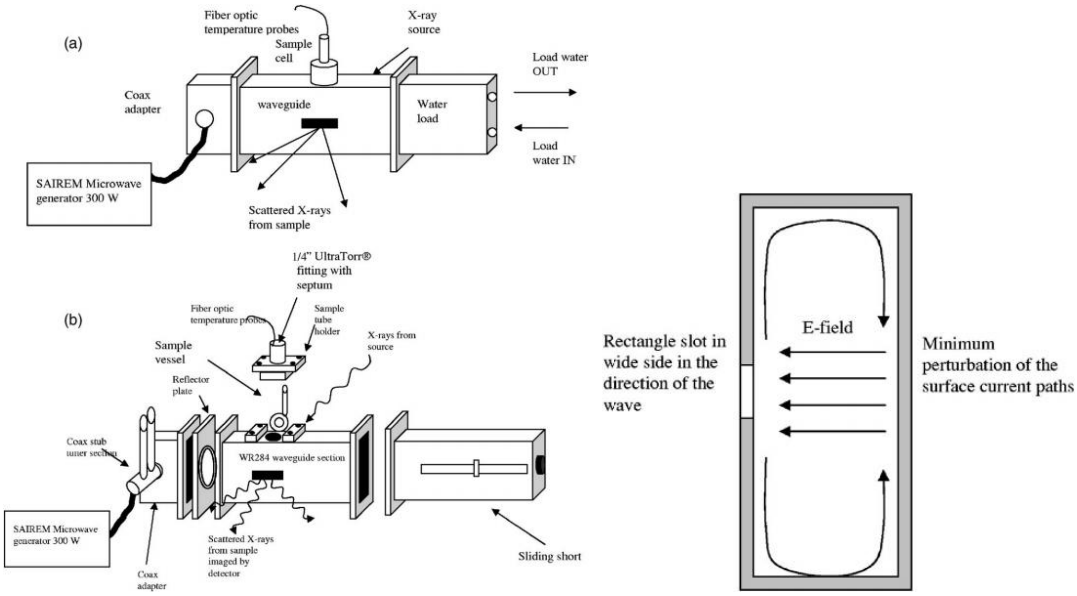

Figure 12a (left). Schematic of in situ SAXS and WAXS microwave synthesis waveguide apparatus, (a) setup 1 with water load and (b) setup 2. Schematic shows an expanded view of the components, which are bolted together at the rectangle flanges. Figure 12b (right). Schematic of the surface current in a waveguide cross section with a slot in the wide side. Reprinted from [4], Copyright (2022), with permission from Elsevier.

Similar work can be found in [33][34].

Conclusion

From the information offered by SAXS and WAXS, outline information can be obtained, such as size, shape or morphology, surface and interaction between entities. However, due to the limited Q (momentum transfer) range, real-space resolution as to bonding information can't be provided. The most advantageous property is in-situ and time-resolution and the combination with other characterization techniques like Raman spectroscopy, FTIR, DSC, DTA, etc. because of its non-invasive nature.

In terms of the information needed for catalysis, the monitoring of the growth and aggregation of nanoparticles during synthesis, reaction, or deactivation processes is of great importance especially in industrial processes or in extreme conditions. The fact that the scattering experiments can be performed in laboratory-based sources and setups increases the feasibility.

The hierarchical structure of information that is offered by the combination of SAXS and WAXS indicates its applicability in such systems with multiple scales. There is great potential in the application of supported heterogeneous catalysts with delicate

design.

References

[1] Terrill1, N. J, Dent1, A. J, Dobson, B. et al. Past, present and future—sample environments for materials research studies in scattering and spectroscopy, a UK perspective; J. Phys.: Condens. Matter 33 (2021) 483002

[2] Benmore, C. J., Robinson, D., Jennings, G., Ilavsky, J. et al. Extended range X-ray pair distribution functions; Nuclear Inst. and Methods in Physics Research, A 955 (2020) 163318

[3] Nørskov, J., Bligaard, T., Rossmeisl, J. et al. Towards the computational design of solid catalysts. Nature Chem 1, 37–46 (2009). https://doi-org.proxy-ub.rug.nl/10.1038/nchem.121

[4] Tompsetta, G. A., Panzarella, B., Conner, W. C..In situ small angle x-ray scattering, wide angle x-ray scattering, and Raman spectroscopy of microwave synthesis. Review of Scientific Instruments 77, 124101 (2006); https://doi-org.proxy-ub.rug.nl/10.1063/1.2390630

[5] Farrowa, C. L., Billinge, S. J. L.. Relationship between the atomic pair distribution function and small-angle scattering: implications for modeling of nanoparticles. Acta Cryst. (2009). A65, 232–239

[6] Fritz-Popovski, G., Bergmanna, A., Glatter, O.. Real space functions from experimental small angle scattering data. Phys. Chem. Chem. Phys., 2011, 13, 5872–5880

[7] Billinge, S. J. L. and Kanatzidis, M. G.. Beyond crystallography: the study of disorder, nanocrystallinity andcrystallographically challenged materials with pair distribution functions. Chem. Commun., 2004, 749–760.

[8] Glatter, O., Kratky, O.. Small Angle X-ray Scattering. John Wiley & Sons, Ltd, 1982.

[9] Bowron1, D. T., Soper, A. K., Jones, K. et al. NIMROD: The Near and Inter Mediate Range Order Diffractometer of the ISIS second target station. Review of Scientific Instruments 81, 033905 (2010); https://doi.org/10.1063/1.3331655

[10] Ryan, A. J., Bras, W., Mant, G. R. and Derbyshire, G. E.. A direct method to determine the degree of crystallinity and lamellar thickness of polymers: application to polyethylene. POLYMER Volume 35 Number 21 1994 4537

[11] Tsubaki, K., Ishizu, K.. Synthesis and solution properties of cylinder brushes derivated by internal domain locking of poly(diblock macromonomer)s. POLYMER Volume42 Issue20 Page8387-8393 DOI10.1016/S0032-3861(01)00347-0

[12] Sota, N., Hashimoto, T.. Process and kinetics of order-order transition from bcc-sphere to hex-cylinder in polystyrene-block-polyisoprene-block-polystyrene: Time-resolved SAXS and TEM studies. POLYMER Volume46 Issue23 Page10392-10404
DOI10.1016/j.polymer.2005.08.038

[13] Tomita, S., Sasaki, S., Sakurai, S.. Time-resolved 2d-SAXS measurements to reveal mechanism of cylinder orientation upon sphere-to-cylinder transition under a planar flow in an SEBS triblock copolymer sheet. EUROPEAN POLYMER JOURNAL

Volume93 Page382-389 DOI10.1016/j.eurpolymj.2017.05.033
[14] Saidi, S.; Portale, G.; Bras, W.; Longo, A.; Amigo, J.M.; Chapron, D.; Bourson, P.; Hermida-Merino, D. Data Mining of Polymer PhaseTransitions upon Temperature Changes by Small and Wide-Angle X-ray Scattering Combined with Raman Spectroscopy. Polymers 2021,13, 4203. https://doi.org/10.3390/polym13234203
[15] Lovinger, A.J. Ferroelectric Polymers. Science 1983, 220, 1115–1121.
[16] Bryant, G. K., Gleeson, H. F., Ryan, A. J., Fairclough, J. P. A. et. al. Raman spectroscopy combined with small angle x-ray scattering and wide angle x-ray scattering as a tool for the study of phase transitions in polymers Review of Scientific Instruments 69, 2114 (1998); https://doi-org.proxy-ub.rug.nl/10.1063/1.1148907
[17] Sreenivas Kummara, Kohji Tashiro. Isotope effect on the structural evolution process in the isothermal crystallization phenomenon of polyoxymethylene. Polymer 90, 76-88.
[18] Wim Bras, Satoshi Koizumi, Nicholas J Terrill. Beyond simple small-angle X-ray scattering: developments in online complementary techniques and sample environments. IUCrJ 1:6, 478-491.
[19] Kohji Tashiro, Hiroko Yamamoto, Taiyo Yoshioka, et.al. Hierarchical Structural Change in the Stress-Induced Phase Transition of Poly(tetramethylene terephthalate) As Studied by the Simultaneous Measurement of FTIR Spectra and 2D Synchrotron Undulator WAXD/SAXS Data. Macromolecules 47:6, 2052-2061.
[20] Garcia, P.R. A. F., Epple, M. , Oliveira, C. L. P. et al. An in situ SAXS investigation of the formation of silver nanoparticles and bimetallic silver–gold nanoparticles in controlled wet-chemical reduction synthesis. Nanoscale Adv., 2020, 2, 225–238.
[21] Juelsholt, M ., Quinson, J., Jensen, K. M. Ø. et al. Surfactant-free syntheses and pair distribution function analysis of osmium nanoparticles. Beilstein J. Nanotechnol. 2022, 13, 230–235. https://doi.org/10.3762/bjnano.13.17
[22] Cheng-Si Tsao and Tsang-Lang Lin. An improved small-angle X-ray scattering analysis of δ' precipitation in an Al-Li alloy for growth kinetic studies. Journal of Applied Crystallography (1999). 32 , 426-435
[23](i) Glatter, O. (1977). J. Appl. Cryst.10, 412-415
(ii) Glatter, O. (1980a).J. Appl. Cryst.13, 7-11
(iii) Glatter, O. & Kratky, O. (1982). Small-Angle X-ray Scattering. London: Academic Press
[24] Singh, A., Vihinen, J., Frankberg, E. et al. Pulsed Laser Ablation-Induced Green Synthesis of TiO2 Nanoparticles and Application of Novel Small Angle X-Ray Scattering Technique for Nanoparticle Size and Size Distribution Analysis. Nanoscale Res Lett 11, 447 (2016). https://doi.org/10.1186/s11671-016-1608-1
[25] Singh, M., Sinha, I., Singh, A.K. et al. Correlating SAXS analysis with LSPR behavior: poly(vinyl alcohol)-stabilized Ag nanoparticles. J Nanopart Res 13, 4387–4394 (2011). https://doi-org.proxy-ub.rug.nl/10.1007/s11051-011-0388-x
[26] Koerner, H., Park, K. et al. In Situ UV/Vis, SAXS, and TEM Study of Single-Phase Gold Nanoparticle Growth. Chem. Mater. 2012, 24, 6, 981–995
[27] Seibt, S., Zhang, H., Mulvaney, P. et al. Growth of Gold Nanorods: A SAXS

Study. J. Phys. Chem. C 2021, 125, 19947−19960
[28] Kuttner, C., Förster, S., Perez-Juste, J., Contreras-Caceres, R. et al. Seeded Growth Synthesis of Gold Nanotriangles: Size Control, SAXS Analysis, and SERS Performance. ACS Appl. Mater. Interfaces 2018, 10, 11152−11163 https://pubs.acs.org/doi/10.1021/acsami.7b19081
[29] Moreau, L. M., Mirkin, C. A., Bedzyk, M. J. et al. How Ag Nanospheres Are Transformed into AgAu Nanocages. J. Am. Chem. Soc. 2017, 139, 35, 12291–12298
[30] Lyu, J., Hamon, C., Constantin, D. et al. Determining the morphology and concentration of core–shell Au/Ag nanoparticles. Nanoscale Adv., 2020,2, 4522-4528.
[31] Vijay, A., Kaur, Ashwinder., Vaidya, S. Synergistic Role of Model-Independent and Model-Dependent Approaches for Determining Size and Shape of Au Nanostructures Using SAXS. Part. Part. Syst. Charact. 2022, 2100285. https://doi-org.proxy-ub.rug.nl/10.1002/ppsc.202100285
[32] Goestena, M. G., Gascon, J . et al. Small-angle X-ray scattering documents the growth of metal-organic frameworks. Catalysis Today 205 (2013) 120–127 http://dx.doi.org/10.1016/j.cattod.2012.08.044
[33] Segovia, G. M., Allegretto, J. A., Azzaroni, O., Rafti, M. et al. Post-synthetic modification and chemical modulation of the ZIF-8 MOF using 3-mercaptopropionic acid (MPA): a multi-technique study on thermodynamic and kinetic aspects. Mol. Syst. Des. Eng., 2022,7, 101-111
[34] Goesten, M. G., Gascon, J. et al. Small-angle X-ray scattering documents the growth of metal-organic frameworks. Catalysis Today 205 (2013) 120–127